# Ribosomal Crystallography: From Poorly Diffracting Microcrystals to High-Resolution Structures

Marco Gluehmann,* Raz Zarivach,† Anat Bashan,† Joerg Harms,*
Frank Schluenzen,* Heike Bartels,*,† Ilana Agmon,† Gabriel Rosenblum,†
Marta Pioletti,‡,§ Tamar Auerbach,†,§ Horacio Avila,‡,¶ Harly A.S. Hansen,*
François Franceschi,‡ and Ada Yonath*,†,1

*Max Planck Research Unit for Ribosomal Structure, Notkestrasse 85, 22603 Hamburg, Germany;
†Department of Structural Biology, Weizmann Institute, 76100 Rehovot, Israel;
‡Max-Planck-Institut für Molekulare Genetik, Ihnestrasse 73, 14195 Berlin, Germany;
§FB Biologie, Chemie, Pharmazie, Frei University Berlin, Takustrasse 3, 14195 Berlin, Germany; and
¶Centro de Investig. Biomédicas, Univ. de Carabobo, Las Delicias, Maracay, Venezuela

The cellular organelles translating the genetic code into proteins, the ribosomes, are large, asymmetric, flexible, and unstable ribonucleoprotein assemblies, hence they are difficult to crystallize. Despite two decades of intensive effort and thorough searches for suitable sources, so far only three crystal types have yielded high-resolution structures: two large subunits (from an archaean and from a mesophilic eubacterium) and one thermophilic small subunit. These structures have added to our understanding of decoding, have revealed dynamic aspects of the biosynthetic process, and have indicated the strategies adopted by ribosomes for interacting between themselves as well as with inhibitors, factors and substrates.   © 2001 Elsevier Science

Ribosomes are the universal cellular organelles catalyzing the sequential polymerization of amino acids according to the genetic blueprint encoded in the mRNA. They are composed of two subunits that associate for accomplishing the synthesis of proteins. The larger subunit creates the peptide bonds, provides the path along which the nascent protein chains emerge from the ribosome, and participates in mRNA/tRNA translocation. The smaller subunit has key roles in the initiation of the process; in decoding the genetic message; in discriminating against cognate and non- and near-cognate aminoacylated tRNA molecules; in controlling the fidelity of codon–anticodon interactions; and in mRNA/

tRNA translocation. The prokaryotic large ribosomal subunit (called 50S) has a molecular mass of $1.5 \times 10^6$ Da. It contains two RNA chains (called 23S and 5S) with a total of about 3000 nucleotides and about 35 proteins. The small ribosomal subunit (called 30S) has a molecular mass of $8.5 \times 10^5$ Da and contains one RNA chain of more than 1500 nucleotides and 20 proteins.

As subjects for crystallographic studies, ribosomes present a long list of concerns resulting from their enormous size; the lack of internal symmetry; the high level of their complexity; their natural tendency to deteriorate and disintegrate; their internal flexibility; their significant conformational variability; and their severe radiation sensitivity. The key to obtaining crystals suitable for crystallographic studies is to use relatively robust ribosomes. An alternative strategy is to crystallize complexes of ribosomes with substrates or factors that are supposed to trap them at preferred orientations. The first three-dimensional crystals obtained from large ribosomal subunits were from *Bacillus stearothermophilus* (1), a source considered to be almost an extremophile at the beginning of the 1980s. Later, crystals of a complex of the whole ribosome with an mRNA/tRNA analog were grown (2). Inbetween, more than 20 crystal types were obtained from ribosomal particles, their complexes mimicking defined stages in protein biosynthesis, and their mutated, selectively depleted, and chemically modified subunits, but only a few of these were suitable for crystallographic analysis (for review see (3)).

---

[1] To whom correspondence should be addressed at the Weizmann Institute. Fax: −972-8-9344154. E-mail: ada.yonath@weizmann.ac.il.

Among the many crystal types grown so far (4), only two types of large ribosomal subunits and one of the small subunits diffract to 3 Å or higher. Although all suffer from severe radiation sensitivity and low isomorphism (4), far beyond the initial expectations, high-resolution structures of these three crystal forms (5–8) and a medium-resolution structure of the whole 70S ribosome were determined (9). These structures, as well as those obtained from complexes of the ribosomal subunits with antibiotics, substrate analogs, and initiation factors (10–16), indicate that decoding and peptide bond formation functions are performed mainly by the ribosomal RNA, and opened the door to further functional insights.

In this article we present our approaches to ribosomal crystallography. We discuss the interplay between crystal structure and the conditions used for crystallization, crystal treatment, and crystal storage. We demonstrate methods that allow control of the conformation of the crystallized particles and show the influence of nonribosomal compounds on the quality of the crystals and, consequently, on the emerging structures. As our phasing strategy is connected in some cases, to crystal stabilization, we have dedicated part of the article to this point.

## THE LARGE RIBOSOMAL SUBUNIT: CRYSTAL GROWTH AND STABILIZATION UNDER CONDITIONS CLOSE TO AND FAR FROM THE PHYSIOLOGICAL ENVIRONMENT

The first diffraction patterns that extended beyond 3-Å resolution were obtained from crystals of large subunits from *Haloarcula marismortui* (H50S), a bacterium that lives in the Dead Sea, the lake with the highest salinity in the world. This bacterium has developed a sophisticated system to accumulate enormous amounts (3–5 M) of KCl, although the Dead Sea contains only milimolar amounts (17). The reasons for the potassium intake are, most probably, not related to ribosome function. Yet, the ribosomes of this bacterium had to adapt to the *in situ* environment, and it was found that their functional activity is directly linked to the concentration of potassium ions in the reaction mixture (Fig. 1).

Initially we grew the crystals of H50S under conditions mimicking the interior of the bacteria at their log period. We used solutions containing all salts required for maintaining a high functional activity of the halophilic ribosomes, including 3 M potassium chloride. Un-

der these conditions, nucleation occurred rapidly and yielded small disordered crystals. Consequently, we developed a procedure for crystallization at the lowest potassium concentration required for maintaining the integrity of the subunits. Once the crystals grew, we transferred them to solutions containing around 3 M KCl, so that the crystallized particles could rearrange into their active conformation and regain their full functional activity. The crystals so obtained exhibited functional activity and diffracted well to high resolution (3, 17), but the high potassium concentration within these crystals (2.8–3.0 M) caused severe problems in the course of structure determination (4). The combination of severe nonisomorphism, apparent twinning, high radiation sensitivity, unstable cell constants, nonuniform mosaic spread, and uneven reflection shape hampered the collection of data usable for structure determination. As these problems became less tolerable at higher resolution, the structure determination under close to physiological conditions stalled at resolutions around than 5-Å (4, 18–20).

After several years of extensive trials, improved crystals were obtained by replacement of the KCl with NaCl and a drastic reduction in the concentration of the salts in the crystal-storage solution (from the original ~3 M KCl to ~1.5 M NaCl), accompanied by a significant increase in the concentration of the organic materials that are present in the crystal-storage solution (double the amount of polyethylene glycol, from 6 to 12%, and of the cryoprotectant ethylene glycol, from 8–18% to more than 22%) (5). These crystals yielded an extremely good electron density map at 2.4-Å resolution (5), in which several functionally relevant key features are disordered. These include the most prominent features of the typical shape of the large subunit, the two lateral protuberances called the "L1 stalk," and "L12 stalk" which are involved in factor-dependent GTPase activity, in translocation, and in the release of the tRNA molecules (for review see (21, 22)).

Most of the structural elements that are disordered in the 2.4-Å (5) structure of H50S were detected in the 5.5-Å (9) maps of the assembled 70S ribosome. This stimulated the notion that features that interact with the small subunit or with ribosomal substrates are disordered in the unbound large subunit, and become stabilized in the 70S ribosome by the intersubunit interactions or by their contacts with the tRNAs. Indeed, biochemical, functional, and electron microscopical studies indicated that these features are inherently flexible. However, flexibility is not necessarily synonymous with disorder. In many cases, flexible structural elements assume several well-defined conformations,

and the switch from one conformation to another is related to their functional states. Detecting large disordered features in a high-resolution structure may indicate that introducing disorder in relevant features is a common ribosomal strategy to avoid unproductive subunit association and substrate binding. Hence, the cause for the disorder of the functionally relevant features in the 2.4-Å structure of H50S (5) may be linked to the fact that these ribosomal particles were measured under conditions very far from the *in situ* situation.

To further investigate this intriguing question, we continued our efforts to elucidate the structure of H50S under close to physiological conditions. Despite the problems of this system, recently we obtained an electron density map from data collected from H50S crystals that were grown and kept under conditions mimicking the physiological environment of *H. marismortui* (I. Agmon, unpublished). The resolution (3.6-Å) of this map is lower than that obtained for the crystals kept under far from physiological conditions (5); nevertheless, the map is interpretable and has enabled a rather detailed comparison between the two structures.

The largest differences were observed in the locations and the internal order of the terminus extensions. Under close to physiological conditions more tails and extensions reach functionally important locations, such as tRNA binding sites and intersubunit bridges. Also, a higher order was seen for many of the RNA regions that are disordered in the 2.4-Å map of H50S (5), such as helices H1 and H38 and the L11 arm. Thus, it is conceivable that the disorder of the features in the 2.4-Å structure of H50S reflects a strategy that the large subunit has developed to avoid nonproductive association with the small subunit or with factors and substrates, under nonnatural conditions.

*H. marismortui* is an archaean bearing low compatibility with *Escherichia coli*, the species yielding most of our knowledge on ribosomes. Despite the suitability of the ribosomes from *H. marismortui* for high-resolution crystallography, they have not been the subject of many biochemical studies. Consequently, only a small part of the vast amount of data accumulated over almost half a century of ribosomal research can be related directly to its structure. In addition, the halophilic cells are rather resistant to most of the antibiotic agents, among them the macrolide family. The latter hardly binds, since a key adenine is a guanine in the halophilic 23S RNA. Thus, it is not surprising that contrary to the wealth of crystallographic information already obtained about binding of factors and antibiotics to the small subunit (11–15), so far only complexes of H50S with compounds believed to represent substrate analogs have been found suitable for high-resolution crys-

tallographic studies (10). Furthermore, the tentative mechanism that was proposed based on the 2.4-Å structure (10) was challenged biochemically (23, 24) and it was shown that all nucleotides that are crucial for the catalytic activity in the proposed mechanism (10) undergo conformational rearrangments as a result of small changes in monovalent ions (24). Also, they can be mutated with little or no effect on peptide bond formation, *in vitro* (25) and *in vivo* (26).

We therefore initiated studies on crystals of the large ribosomal subunit from a robust mesophilic eubacterium, *Deinococcus radiodurans* (D50S), which were grown and maintained under close to the physiological conditions (8). The ribosome from this source shows a high homology to those of *Thermus thermophilus* and *E. coli*, and the crystals of its large subunit were grown and maintained under conditions that are almost identical to those of the bacteria *in situ* environment. These crystals, as well as those grown from their complexes with antibiotics and substrate analog, diffract to higher than 3-Å resolution and are relatively stable in the X-ray beam. Thus, they provide an excellent system to shed light on the mechanism of peptide bond formation and to investigate antibiotic binding, which should lead to rational drug design.

Analysis of the 3-Å structure of D50S (Fig. 2) opened the gate to a better understanding of functional flexibility. Thus, most of the features that are disordered in H50S are resolved in the 3-Å structure (Fig. 2) of D50S. These include the intersubunit bridge (H69) connecting the large subunit to the decoding center in the small subunit and the middle loop of protein L5 that forms the "only protein" bridge. It also contains the entire L1 stalk (helices H76–H78), the GTPase center (helices H42–H44 and protein L11), and a significant part of the so-called "A finger (H38)." All show orientations that differ, to various extents, from those seen in the 5.5-Å structure of the *T. thermophilus* 70S (T70S) ribosome complex (9), manifesting their inherent flexibility.

Figure 3 demonstrates a feasible sequence of events leading to the creation of the intersubunit bridge from the large subunit to the decoding center on the small one. Helix H69, which is responsible for this bridge, lies in the unbound 50S subunit on the interface surface and interacts intensively with helix H70. Once the initiation complex, which includes the small subunit and tRNA at the P site (see below for more detail), approaches the large subunit, the tRNA pushes helix H69 toward the decoding center, and the intersubunit bridge is formed.

The inherent flexibility of the ribosomal features may also be exploited for controlling events during translocation. The comparison between the structure of the

unbound D50S and the T70S ribosome hints how the L1 arm may facilitate the exit of the tRNA molecules. In the complex of T70S with three tRNA molecules, the L1 stalk interacts with the elbow of E-tRNA and the exit path for the E-tRNA is blocked by proteins L1 from the large subunit and S7 from the small subunit (9). In the unbound mesophilic D50S, the L1 arm is tilted by about 30° away from its position in the T70S ribosome (Fig. 3). Superposition of the structure of mesophilic unbound D50S on the entire ribosome allowed definition of a pivot point for a possible rotation of the L1 arm, and showed that in this orientation it would not block the presumed exit path of the E-site tRNA (8). Hence, it is likely that the mobility of the L1 arm is used for facilitating the release of E-site tRNA.

## THE SMALL RIBOSOMAL SUBUNIT: THE CONNECTION BETWEEN CRYSTAL TREATMENT, BETTER ISOMORPHISM, AND HIGHER RESOLUTION

The small ribosomal subunit is less stable than the large one. We found that by exposing 70S ribosomes to a potent proteolytic mixture, the 50S subunits remained intact, whereas the 30S subunits were completely digested. Similarly, crystals obtained from 70S ribosomes assembled from purified subunits were found to consist only of 50S subunits (3), and the supernatant of the crystallization drop did not contain intact small subunits, but its proteins and fragmented 16S RNA chains.

**FIG. 1.** Functional activity of the ribosomes from *H. marismortui* at different potassium concentrations. Activity was checked by the synthesis of polypeptides, and by the incorporation of 50S into 70S. In both cases the ribosomal particles underwent activation at 55°C for 40 min, and homo- or heteronucleotides served as mRNA chains.
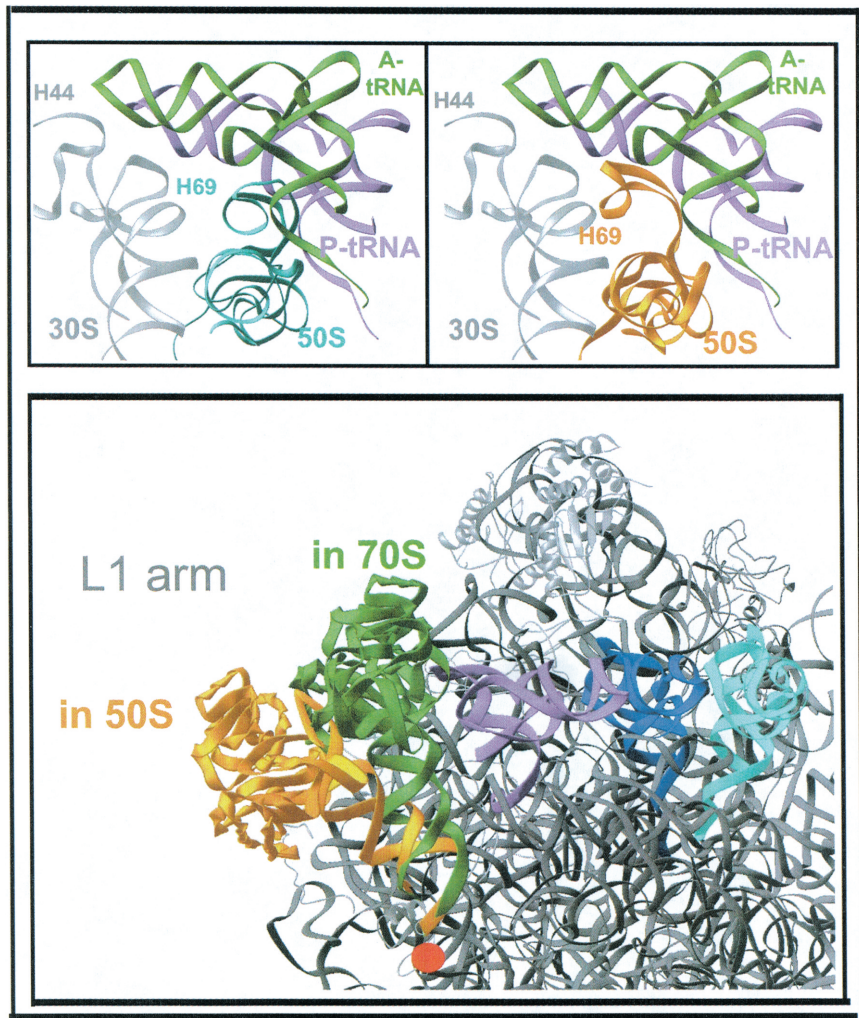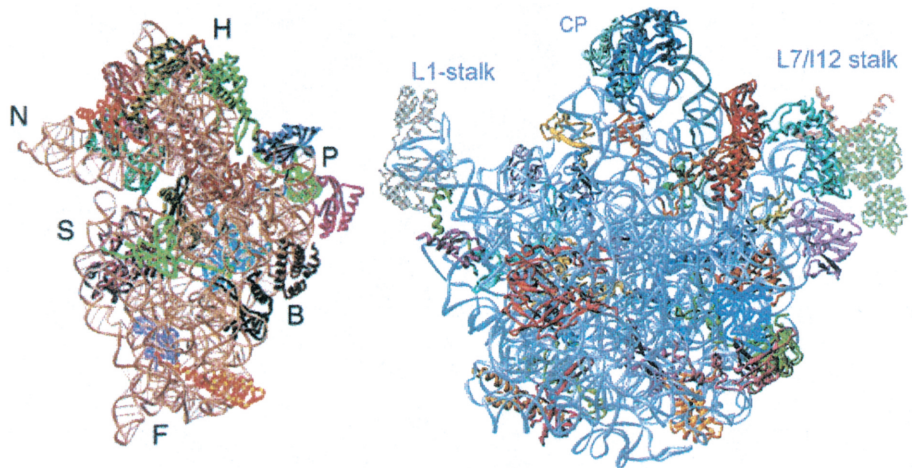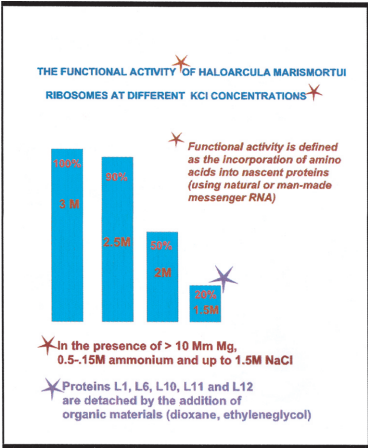
**FIG. 2.** Three-dimensional structures of the small (left) and large (right) ribosomal subunits, both shown from their interface sides. Landmarks: Small subunit: H, head; B, body; P, platform; S, shoulder; N, nose; F, foot. Large subunit: L1 stalk; L7/12 stalk, GTPase stalk; CP, central protuberance. This figure was created using RIBBONS (54).
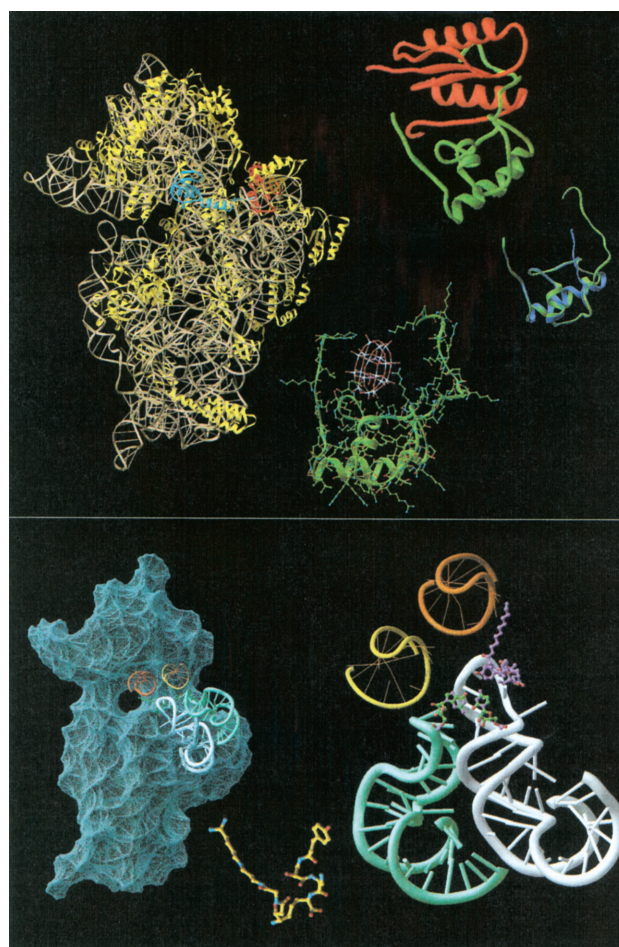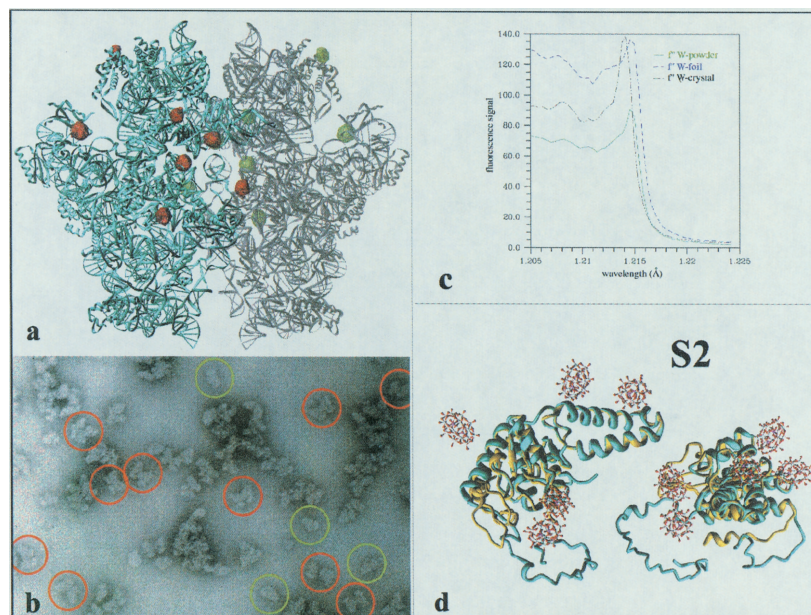
**FIG. 3.** Intersubunit bridge formed by helix H69. *Top*: The small subunit is placed on the left side and the large subunit on the right. Helix H44 of the small subunit is shown in gray. Also shown are the docked tRNA molecules (P-site tRNA in magenta and A-site tRNA in green). Coordinates of the docked small subunit and the two tRNA sites were taken from (9). For clarity, the mRNA is not shown. The top left-hand box shows the shape of H69 in unbound D50S. In this position H69 interacts with its neighbors in the 50S subunit. On association with the initiation complex the P-site tRNA pushes H69 toward the small subunit, until it reaches its bound conformation (in gold), as determined in the 70S complex (9). *Bottom*: Part of the upper side of the view shown in Fig. 2 (right), with the L1 stalk on the left. The gold feature represents its position in unbound D50S, and the green, in the whole ribosome (T70S). Red indicates a possible pivot point. In the complex of the whole ribosome with three tRNA molecules (9), this arm assumes a conformation that may correspond to a "closed-gate" trapping the E-site tRNA (magenta). For orientation, the P-site (blue) and the A-site (cyan) tRNAs are also shown. The conformation seen in the unbound 50S subunit may represent the "open-gate" state. This figure was created using RIBBONS (54).

**FIG. 4.** W18, its phasing contribution and its position within the crystals of T30S. (a) Locations of W18 clusters (shown as green and red balls) that bind to two 30S subunits (in gray and in cyan, respectively) related by a crystallographic twofold axis. The figure reflects the situation at 3.8-Å resolution, when about 90% of the proteins and RNA were traced. (b) Content of carefully dissolved crystals of tungstenated T30S, as seen by EM (negative staining). Typical butterfly shape of T30 apparent dimers (reminiscent of the crystalline network around the twofold axes) are shown within red circles, and single particles are circled in green. (c) Anomalous X-ray scattering of the W18 cluster. $f''$ as a function of wavelength, as derived from fluorescence spectra measured from a W foil, W powder, and a crystal soaked in a W18 solution, all measured around the W $L_{III}$ edge. (d) Two views of protein S2, the protein that binds the largest number of W18 clusters. The W18-bound protein is shown in cyan and the free in (PDB code: 1FJF) in yellow. The W atoms within the W18 clusters that are bound to the protein are shown in red. Panels showing structural elements were created using RIBBONS (54).

**FIG. 5.** *Top left*: Location of IF3 on the small subunit (same view as in Fig. 2). IF3C is shown in red and I3FN in blue. *Top middle*: Binding of IF3C (red) and of W18 (white–red ellipsoid) by protein S18 (green) is shown on top and bottom, respectively. *Top right*: For comparison, protein S18 in the IF3C-bound state is overlaid on the same protein in the nontungstenated structure (7). *Bottom*: Binding of the universal antibiotic edeine to the small subunit. *Bottom left*: Overall view (color code of the helical elements as described below). The small subunit is shown at about 75° rotation (around the vertical axis of the particle) compared with the view on top. The mRNA channel is clearly seen and the sites P (orange) and E (yellow) are indicated. *Bottom right*: Closeup of edeine binding area. H23 is shown in light green and H24 in white. Edeine is pink, and the newly formed base pair is green. The inhibitory action of this antibiotic interfering with the initiation process by limiting the mobility of the platform is evident. *Bottom middle*: Structure of edeine. This figure was created using RIBBONS (54).

THE FUNCTIONAL ACTIVITY OF HALOARCULA MARISMORTUI
RIBOSOMES AT DIFFERENT KCl CONCENTRATIONS

Functional activity is defined
as the incorporation of amino
acids into nascent proteins
(using natural or man-made
messenger RNA)

In the presence of > 10 Mm Mg,
0.5-.15M ammonium and up to 1.5M NaCl

Proteins L1, L6, L10, L11 and L12
are detached by the addition of
organic materials (dioxane, ethyleneglycol)

Because of its lower stability, the small ribosomal sub-unit seemed to be hardly suitable for crystallographic studies. Indeed, contrary to the marked tendency of large subunits to crystallize, only one crystal form has so far been obtained from the small subunit (27, 28). For almost a decade this crystal form, T30S, yielded satisfactory data only to 7–9 Å, hence various approaches in pre and postcrystallization treatment have been developed for improving the quality of the diffraction from T30S crystals.

The severe nonisomorphism of the T30S crystals was minimized by several approaches. One of them is postcrystallization addition of metal hexammines (29). Hexammines are known to bind specifically to RNA chains in a way that may increase their rigidity; therefore they were used to generate a large number of high-quality crystals of several RNA compounds, such as the ribozyme domains P4–P6, for which cobalt(III) hexammine chloride dramatically increased the number, size, and growth rate of the crystals (30). Better diffraction and higher isomorphism were also reported for spectinomycin-bound 30S crystals (11). This antibiotic agent was shown to lock the 30S head in a particular conformation and it seems that this improved the quality of the crystals. Additional materials that hinder internal motions are multimetal clusters (31). Although the mechanism for minimizing internal motions may differ in the various systems, the resulting fixation of the conformation seems to lead to a similar improvement in crystal properties.

The stabilization of T30S crystals by large metal clusters was based on the following findings: (a) the crystals contain a large continuous solvent region; (b) the small subunits are packed so that the part of their surface that does not interact with 50S and is suggested to be rich in proteins is pointing toward the crystal solvent region. We therefore engineered well-diffracting crystals of T30S by minimizing the conformational heterogeneity and limiting the mobility of the crystallized particles. The crystals were exposed to elevated temperatures, following the routine heat activation procedure (32), and then stabilized by a heteropolytungstate cluster, $[(NH_4)_6(P_2W_{18}O_{62}) \cdot 14H_2O]$ (33), referred to below as W18. This cluster played a dual role, as it also yielded phase information.

Most of the W18 sites that were detected in the electron density maps of the tungstenated crystals interact with ribosomal proteins, in positions that may significantly reduce the global mobility of the T30S particles within the crystal network (Fig. 4). Pairing of T30S particles around the crystallographic twofold axis is one of the main features of the crystallographic network in T30S crystals (19). The contacts holding these pairs are extremely stable, so that they are maintained even after the rest of the crystal network is destroyed. Large proportions of butterfly-shaped pairs have been observed by electron microscopy in samples of thoroughly washed and dissolved T30S crystals (Fig. 4), and it was found that the pairing contacts are formed by the W18 clusters located at the interface between the particles in the electron density map.

The tendency of the heteropolytungstates to bind in relatively narrow solvent regions was detected also in internal cavities of other ribosomal crystals. One of these is the tunnel of the large ribosomal subunit, believed to provide the exit path of the nascent proteins, detected first by three-dimensional image reconstruction using diffraction data obtained from tilt series of two-dimensional sheets of large subunits (34) and 70S ribosomes (35). Its existence was reconfirmed almost a decade later by cryo-electron microscopy (36, 37) as well as by X-ray crystallographic studies (38). Attachment of heteropolytungsten clusters to the inner walls of this tunnel in H50S ribosomal subunits has been observed at 5- to 7-Å resolution (18).

## MULTI-HEAVY-ATOM CLUSTERS ARE USEFUL FOR PHASING AT HIGH RESOLUTION

The assignment of phases to the observed structure factor amplitudes is the most crucial step in structure determination. Since the phases cannot be measured, they are elucidated indirectly. Combinations of isomorphous replacement and anomalous dispersion are the commonly used methods for phasing diffraction data from crystals of biological macromolecules. These require the preparation of heavy atom derivatives in which electron-dense compounds are inserted into the crystalline lattice at distinct locations. As the changes in the structure factor amplitudes resulting from the addition of the heavy atoms are being exploited, the derivatization reagents are chosen according to their potential ability to induce measurable signals (39). In ribosomal crystallography, several heteropolytungstates (40) were found suitable for phasing at low resolution, as well as for the validation of the results obtained by molecular replacement searches: $(Na_{16}[(O_3PCH_2PO_3)_4W_{12}O_{36}] \cdot 40H_2O)$, $(Cs_7(P_2W_{17}O_{61}\text{-}Co(NC_5H_5)) \cdot 14H_2O)$ (4), $[(phSn)_4(AsW_9O_{33})_2]$, $Cs_5[PW_{11}O_{39}[Rh_2CH_3COO_2]$ (18), $H_4SiO_4[12WO]$ and $Li_{10}(P_2W_{17}O_{61})$ (29), $((NH_4)_6(P_2W_{18}O_{62}) \cdot 14H_2O)$, and $((TMA)_2Na_2 [Nb_2W_4O_{19}] \cdot 18H_2O)$ (31).

Among the heavy atoms used by us for MIRAS phasing, the W18 $[(NH_4)_6(P_2W_{18}O_{62}) \cdot 14H_2O]$ cluster (33) has made the most significant contribution. At least 13 such clusters bind rather firmly to each subunit, and since

the spatial arrangement of their components is well defined, their considerable anomalous dispersion was found useful for phasing. At resolutions lower than 4-Å, the W atoms were not resolved and only part of the 13 tungsten clusters that bind to the small subunit could be detected in difference Patterson maps. Hence in the initial stages, phase information was obtained by representing the clusters by their spherically averaged form factor (31). At higher than L1A resolution, we located 13 clusters, and resolved the positions of the individual W atoms within 10 of them. We then used them, together with four additional smaller heavy atoms, for anomalous phasing (2,845,385 observations with completeness of 86.8% (38.2% in the last shell), $R_{sym}$ = 13.6 (38.1), $I/\sigma$ = 19.8(2.0), $R$ = 19.4%, and $R_{free}$ = 25.1%) (6, 14).

The W18 cluster was also found useful for stabilization of the small ribosomal subunit at specific conformations. The first task of the small subunit is to form the initiation complex; therefore we assumed that the commonly used heat-activation procedure, developed over 30 years ago (32), induces the conformation required for this task. To obtain small subunits at that particular conformation, we exposed our T30S crystals to elevated temperatures, according to the standard heat-activation procedure. Once activation was achieved, the conformation of the particles was stabilized (at ambient temperature) by incubation with minute amounts of W18. The same procedure was employed for complexes of T30S with compounds that facilitate or inhibit protein biosynthesis, mRNA analogs, initiation factors, and antibiotics. Soaking in solutions containing the nonribosomal compounds in their normal binding buffer was performed at elevated temperatures. Once the functional complex was formed, the crystals were treated with W18 cluster.

An illuminating example is the structure of T30S in complex with initiation factor 3 (IF3). The initiation of protein biosynthesis has an important role in governing the accurate setting of the reading frame, as it facilitates the identification of the start codon of the mRNA. The initiation complex contains, in prokaryotes, the small subunit, mRNA, three initiation factors, and initiator tRNA. IF3 plays multiple roles in the formation of this complex. It influences the binding of the other ligands and acts as a fidelity factor by destabilizing noncanonical codon–anticodon interactions. It also selects the start mRNA codon (41), stabilizes the binding of the fMet-tRNA/IF2 complex to 30S, discriminates against leaderless mRNA chains (42), and acts as an anti-association factor (43). IF3 is a small basic protein, built of C- and N-terminus domains (IF3C and IF3N, respectively) that are connected by a rather long lysine-rich linker region.

Crystals of the complex of T30S with IF3C were produced by heat activation followed by W18 stabilization. We found that the conformation of the small subunits in this crystals is almost identical to that obtained by heat activation of the isolated particles (14). This indicates that activated and stabilized T30S have the conformation of the small subunit during the initiation phase of protein biosynthesis. It also explains why no major conformational changes were observed between the tungstenated and IF3C-bound 30S subunits. We therefore conclude that the conformation of the tungsten-bound 30S ribosomal subunit, mimics that of the small subunit at the initiation stage and that the W18 cluster imitates the C-terminal domain of IF3 (Fig. 5). Indeed, in competition experiments it was found that crystals that were treated with W18 prior to soaking in solutions containing IF3C failed to bind IF3C.

We found that IF3C binds to the 30S particle at the upper end of the platform on the solvent side (Fig. 5), close to the anti-SD region of the 16S rRNA (14). This location reconfirms the results from NMR and mutagenesis of the IF3 molecule and is compatible with almost all crosslinking, mutation footprints, and protection patterns that were reported for the *E. coli* system (14). The initiator mRNA in prokaryotes includes, along with the start codon, an upstream purine-rich sequence (called SD for Shine–Dalgarno), which pairs with a complementary region in the 16S RNA, at its 3'-end, thus anchoring the mRNA chains. In the high resolution structures of the 30S subunit the anti-SD region is located on the solvent side of the platform, a region that also contains a large part of the E (exit) site and IF3C binding site.

It has been suggested that the C-terminal domain of IF3 (IF3C) performs many of the tasks assigned to the entire IF3 molecule: preventing the association of the 30S with the 50S subunit and contributing to the dissociation of the entire ribosome (44). The ability of IF3 to discriminate noncanonical initiation codons, or to verify codon–anticodon complementarity, has been attributed mainly to IF3N (45). The location of IF3C we observed suggests that the binding of IF3C to the 30S subunit influences the mobility of the platform, near the anchoring site of the SD sequence (46). The spatial proximity of the IF3C binding site to the anti-SD region suggests a connection between IF3 and the interactions of the mRNAs with the anti-SD region. These interactions could suppress the change in the conformational dynamics induced by IF3, thus allowing subunit association.

The binding of IF3C and the hybridization of the anti-SD sequence are likely to limit the mobility of this region. The initial step of protein biosynthesis involves the detachment of the Shine–Dalgarno sequence of the

mRNA. On the detachment of the SD anchor, required at the beginning of the translocation process, the platform may regain its conformational mobility. The bound IF3N leaves a limited, albeit sufficient, space for P-site tRNA, and only small conformational changes are required for simultaneous binding of IF3N, mRNA, and the P-site tRNA. Thus, it seems that the influence of IF3N on initiator tRNA binding is based on space exclusion principles.

Support for the placement of IF3, and for the mechanism inferred from it is provided by the analysis of the mode of action and the location of edeine (Fig. 5), a universal antibiotic agent that interferes with the initiation process (47, 48). Edeine is a peptide-like antibiotic agent containing a spermidine-type moiety at its C-terminal end and a $\beta$-tyrosine residue at its N-terminal end (49). Using crystals of the complex of edeine with T30S, we found that edeine binds in the solvent side of the platform. It also induces the formation of a new base pair between two helices of the platform. In its position, edeine would not alter IF3C binding but might well affect the binding of the linker and, hence, the binding of IF3N. At the same time, it could affect 30S mobility, interaction of the 3′ end with IF3C, and interaction of the 30S and 50S subunits, since it connects the penultimate helix (H44) with the major constituents of the platform. By physically linking these components, edeine can lock the small subunit (Fig. 5) and hinder the conformational changes that accompany the translation process. Independent studies show that pactamycin, an antibiotic agent that shares a protection pattern with edeine, bridges the same helices that are linked by the base pair that is induced by edeine (11).

The universal effect of edeine on initiation implies that the main structural elements important for the initiation process are conserved in all kingdoms. Our results show that the rRNA bases that bind edeine are conserved in chloroplasts, mitochondria, and the three phylogenetic domains. EM studies on rat liver 40S in complex with the eukaryotic initiation factor 3 located it in a region comparable to our findings (50). In this location, IF3 and its eukaryotic counterpart seem to perform their anti-association activity by effecting the conformational mobility of the small ribosomal subunit, in particular suppressing the conformational mobility of the platform, essential for association of the two ribosomal subunits. Some aspects of the initiation process of protein biosyntheses were found to be different in eukaryotic and prokaryotic systems (51). Nevertheless, neither of these indicates different locations of initiation factor 3. The consistency between our results and the location of the eukaryotic initiation factor may indicate that the main concepts underlying the initiation process and governing the anti-association properties of the initiation complex have been evolutionarily conserved.

## IS DISORDER OF FUNCTIONAL ELEMENTS A COMMON RIBOSOMAL STRATEGY?

Almost all ribosomal proteins are built of globular domains with extended tails or loops. Most of the globular domains are located on the solvent side of the particle, whereas the long tails are buried in the interior of the particle, and seem to stabilize the RNA fold. A few proteins have tails pointing into the solution and are less engaged in RNA contacts. Some of these may make crucial contributions to the efficient binding of nonribosomal factors participating in the process of protein biosynthesis, by using their long tails to enhance the correct positioning of these factors (14).

Striking differences in the conformations of the proteins that bind IF3 (S18, S11, and S7) and of those proteins that interact with the binders (e.g. S2) were detected by comparing the structure of unbound T30S with that of IF3-bound T30S (Figs. 4, 5). These proteins belong to the group with tails pointing toward the solution. An interesting example is protein S18. Its long terminus tail is disordered in unbound T30S, but ordered in the tungstenated or IF3C-bound particle. It is conceivable that these tails act as tentacles that enhance the binding of IF3C, consistent with the firm binding of this domain to the ribosome (52, 53). They are also capable of binding IF3C mimics, such as the W18 cluster (Fig. 5). Furthermore, since the protein tails can become disordered, it is possible that the flexibility of these tails is used for the reverse action: the release of the factor once its binding is no longer required.

These results, together with the observation that functionally relevant features are disordered in large subunits (H50S) investigated under nonphysiological conditions, but are well ordered under conditions optimized for maximum activity, suggest that the ribosome has developed a common strategy for preventing nonproductive binding of factors and substrates, as well as minimizing the intersubunit association when conditions are not suitable for efficient protein biosynthesis.

# REFERENCES

1. Yonath, A., Mussig, J., Tesche, B., Lorenz, S., Erdmann, V., and Wittmann, H.G. (1980) *Biochem. Int.* **1,** 428.

2. Hansen, H. A. S., Volkmann, N., Piefke, J., Glotz, C., Weinstein, S., Makowski, I., Meyer, S., Wittmann, H. G., and Yonath, A. (1990) *Biochim. Biophys. Acta* **1050,** 1–7.

3. Berkovitch-Yellin, Z., Bennett, W. S., and Yonath, A. (1992) *Crit. Rev. Biochem. Mol. Biol.* **27,** 403–444.

4. Yonath, A., Harms, J., Hansen, H. A. S., Bashan, A., Schlunzen, F., Levin, I., Koelln, I., Tocilj, A., Agmon, I., Peretz, M., Bartels, H., Bennett, W.S., Krumbholz, S., Janell, D., Weinstein, S., Auerbach, T., Avila, H., Piolleti, M., Morlang, S., and Franceschi, F. (1998) *Acta Crystallogr.* **54,** 945–955.

5. Ban, N., Nissen, P., Hansen, J., Moore, P., and Steitz, T. (2000) *Science* **289,** 905–920.

6. Schluenzen, F., Tocilj, A., Zarivach, R., Harms, J., Gluehmann, M., Janell, D., Bashan, A., Bartels, H., Agmon, I., Franceschi, F., and Yonath, A. (2000) *Cell* **102,** 615–623.

7. Wimberly, B., Brodersen, D., Clemons, W., Morgan-Warren, R., Carter, A., Vonrhein, C., Hirtsch, T., and Ramakrishnan, V. (2000) *Nature* **407,** 327–339.

8. Harms, J., Schluenzen, F., Zarivach, R., Bashan, A., Gat, S., Bartels, H., Agmon, I., Franceschi, F., and Yonath, A. (2001) *Cell* **107,** 1–20.

9. Yusupov, M. M., Yusupova, G. Z., Baucom, A., Lieberman, K., Earnest, T. N., Cate, J. H., and Noller, H. F. (2001). *Science* **292,** 883–896.

10. Nissen, P., Hansen, J., Ban, N., Moore, P. B., and Steitz, T. A. (2000) *Science* **289,** 920–930.

11. Carter, A., Clemons, W., Brodersen, D., Morgan-Warren, R., Wimberly, B., and Ramakrishnan, V. (2000) *Nature* **407,** 340–348.

12. Brodersen, D. E., Clemons, W. M., Carter, A. P., Morgan-Warren, R. J., Wimberly, B. T., and Ramakrishnan, V. R. (2000) *Cell* **103,** 1143–1154.

13. Carter, A. P., Clemons, W. M., Jr., Brodersen, D. E., Morgan-Warren, R. J., Hartsch T., Wimberly, B. T., and Ramakrishnan, V. (2001) *Science* **291,** 498–501.

14. Pioletti, M., Schlünzen, F., Harms, J., Zarivach, R., Glühmann, M., Avila, H., Bashan, A., Bartels, H., Auerbach, T., Jacobi, C., Hartsch, T., Yonath, A., and Franceschi, F. (2001) *EMBO J.* **20,** 1829–1839.

15. Ogle, J. M., Brodersen, D. E., Clemons, W. M., Jr., Tarry, M. J., Carter, A. P., and Ramakrishnan, V. (2001) *Science* **292,** 897–902.

16. Schluenzen, F., Zarivach, R., Harms, J., Bashan, A. Tocilj, A. Albrecht, A. Yonath, A., and Franceschi, F. (2001) *Nature* **413,** 814–821.

17. Von Boehlen, K., Makowski, I., Hansen, H. A. S., Bartels, H., Berkovitch Yellin, Z., Zaytzev Bashan, A., Meyer, S., Paulke, C., Franceschi, F., and Yonath, A. (1991) *J. Mol. Biol.* **222,** 11–16.

18. Ban, N., Nissen, P., Hansen, J., Capel, M., Moore, P.B., and Steitz, T. A. (1999) *Nature* **400,** 841–847.

19. Harms, J., Tocilj, A., Levin, I., Agmon, I., Stark, H., Kölln, I., van Heel, M., Cuff, M., Schlünzen, F., Bashan, A., Franceschi, F., and Yonath, A. (1999) *Struct. Fold. Des.* **7,** 931–941.

20. Weinstein, S., Jahn, W., Glotz, C., Schlunzen, F., Levin, I., Janell, D., Harms, J., Kolln, I., Hansen, H. A. S., Gluhmann, M., Bennett, W. S., Bartels, H., Bashan, A., Agmon, I., Kessler, M., Pioletti, M., Avila, H., Anagnostopoulos, K., Peretz, M., Auerbach, T., Franceschi, F., and Yonath, A. (1999) *J. Struct. Biol.* **127,** 141–151.

21. Franceschi, F., Sagi, I., Boeddeker, N., Evers, U., Arndt, E., Paulke, C., Hasenbank, R., Laschever, M., Glotz, C., Piefke, J., Muessig, J., Weinstein, S., and Yonath, A. (1994) *Syst. Appl. Microbiol.* **16,** 697–705.

22. Sanyal, S. C., and Liljas, A. (2000) *Curr. Opin. Struct. Biol.* **10,** 633–636.

23. Barta, A., Dorner S., and Polacek N. (2001) *Science* **291,** 203–204.

24. Bayfield, M. A., Dahlberg, A. E., Schulmeister, U., Dorner, S., and Barta, A. (2001) *Proc. Natl. Acad. Sci. USA* **98,** 10096–10101.

25. Thompson, J., Kim, D. F., O'Connor, M., Lieberman, K. R., Bayfield, M. A., Gregory, S. T., Green, R., Noller, H. F., and Dahlberg A. E., (2001) *Proc. Natl. Acad. Sci. USA* **98,** 9002–9007.

26. Polacek, N., Gaynor, M., Yassin, A., and Mankin, A. S. (2001) *Nature* **411,** 498–501.

27. Yonath, A., Glotz, C., Gewitz, H. S., Bartels, K. S., von Bohlen, K., Makowski, I., and Wittmann, H. G. (1988) *J. Mol. Biol.* **203,** 831–834.

28. Trakhanov, S. D., Yusupov, M. M., Agalarov, S. C., Garber, M. B., Ryazantsev, S. N., Tischenko, S. V., and Shirokov, V. A. (1987) *FEBS Lett.* **220,** 319–322.

29. Clemons, W. M., Jr, Brodersen, D. E., McCutcheon, J. P., May, J. L. C., Carter, A. P., Morgan-Warren, R. J., Wimberly, B. W., and Ramakrishnan, V. (2001) *J. Mol. Biol.* **310,** 827–843.

30. Cate, J. H., and Doudna, J. A. (1996) *Structure* **4,** 1221–1229.

31. Tocilj, A., Schluenzen, F., Janell, D., Gluehmann, M., Hansen, H. A., Harms, J., Bashan, A., Bartels, H., Agmon, I., Franceschi, F., and Yonath, A. (1999) *Proc. Natl. Acad. Sci. USA* **96,** 14252–14257.

32. Zamir, A., Miskin, R., and Elson, D. (1971) *J. Mol. Biol.* **60,** 347–364.

33. Dawson, B. (1953) *Acta Crystallogr.* **6,** 113–126.

34. Yonath, A., Leonard, K. R., and Wittmann, H. G. (1987) *Science* **236,** 813–816.

35. Arad, T., Piefke, J., Weinstein, S., Gewitz, H. S., Yonath, A., and Wittmann, H. G. (1987) *Biochimie* **69,** 1001–1006.

36. Stark, H., Mueller, F., Orlova, E. V., Schatz, M., Dube, P., Erdemir, T., Zemlin, F., Brimacombe, R., and van Heel, M. (1995) *Structure* **3,** 815–821.

37. Frank, J., Zhu, J., Penczek, P., Li, Y. H., Srivastava, S., Verschoor, A., Radermacher, M., Grassucci, R., Lata, R. K., and Agrawal, R. K. (1995) *Nature* **376,** 441–444.

38. Yonath, A., and Franceschi, F. (1998) *Struct. Fold. Des.* **6,** 679–684.

39. Thygesen, J., Weinstein, S., Franceschi, F., and Yonath, A. (1996) *Structure* **4,** 513–518.

40. Wei, X. Y., Dickman, M. H., and Pope, M. T. (1997) *Inorg. Chem.* **36,** 130–131.

41. Sussman, J. K., Simons, E. L., and Simons, R. W. (1996) *Mol. Microbiol.* **21,** 347–360.

42. Tedin, K., Moll, I., Grill, S., Resch, A., Graschopf, A., Gualerzi, C. O., and Blasi, U. (1999) *Mol. Microbiol.* **31,** 67–77.

43. Grunberg-Manago, M., Dessen, P., Pantaloni, D., Godefroy-Colburn, T., Wolfe, A. D., and Dondon, J. (1975) *J. Mol. Biol.* **94,** 461–478.

44. Hershey, J. W. (1987) *in* ASM Molecular Biology (Neidhardt, F., Ingraham, J., Low, K., Magasanik, B., Schaechter, M., and Umbarger, H., Eds), pp. 613–647, ASM, Washington, DC.

45. Bruhns, J., and Gualerzi, C. O. (1980) *Biochemistry* **19,** 1670–1676.

46. Gabashvili, I., Agrawal, R. K., Grassucci R., and Frank, J. (1999) *J. Mol. Biol.* **286,** 1285–1291.

47. Altamura, S., Sanz, J. L., Amils, R., Cammarano, P., and Londei, P. (1988) *Sys. Appl. Microbiol.* **10,** 218–225.

48. Odon, O. W., Kramer, G., Henderson, A. B., Pinphanichakarn, P., and Hardesty, B. (1978) *J. Biol. Chem.* **253,** 1807–1816.

49. Kurylo-Borowska, Z. (1975) *Biochim. Biophys. Acta* **399,** 31–41.

50. Srivastava, S., Verschoor, A., and Frank, J. (1992) *J. Mol. Biol.* **226,** 301–304.

51. Hershey, J. W., Asano, K., Naranda, T., Vornlocher, H. P., Hanachi, P., and Merrick, W. C. (1996) *Biochimie* **78,** 903–907.

52. Sette, M., Spurio, R., Van Tilborg, P., Gualerzi, C. O., and Boelens, R. (1999) *RNA* **5,** 82–92.

53. Weiel, J., and Hershey, J. W. (1981) *Biochemistry* **20,** 5859–5865.

54. Carson, M. (1997) *Methods Enzymol.* **277,** 493–505.